The Astrophysical Journal Letters, 806:L24 (6pp), 2015 June 20 doi:10.1088/2041-8205/806/2/L24

DISTORTED CYCLOTRON LINE PROFILE IN CEP X-4 AS OBSERVED BY *NuSTAR*

F. Fürst[1], K. Pottschmidt[2,3], H. Miyasaka[1], V. Bhalerao[4], M. Bachetti[5], S. E. Boggs[6], F. E. Christensen[7], W. W. Craig[6,8], V. Grinberg[9], C. J. Hailey[10], F. A. Harrison[1], J. A. Kennea[11], F. Rahoui[12,13], D. Stern[14], S. P. Tendulkar[1], J. A. Tomsick[6], D. J. Walton[1,14], J. Wilms[15], and W. W. Zhang[3]

[1] Cahill Center for Astronomy and Astrophysics, California Institute of Technology, Pasadena, CA 91125, USA
[2] CRESST, Department of Physics, and Center for Space Science and Technology, UMBC, Baltimore, MD 21250, USA
[3] NASA Goddard Space Flight Center, Greenbelt, MD 20771, USA
[4] Inter-University Center for Astronomy and Astrophysics, Ganeshkhind, Pune 411007, India
[5] Osservatorio Astronomico di Cagliari, I-09047 Selargius (CA), Italy
[6] Space Sciences Laboratory, University of California, Berkeley, CA 94720, USA
[7] DTU Space, National Space Institute, Technical University of Denmark, DK-2800 Lyngby, Denmark
[8] Lawrence Livermore National Laboratory, Livermore, CA 94550, USA
[9] Massachusetts Institute of Technology, Kavli Institute for Astrophysics, Cambridge, MA 02139, USA
[10] Columbia Astrophysics Laboratory, Columbia University, New York, NY 10027, USA
[11] Department of Astronomy & Astrophysics, The Pennsylvania State University, University Park, PA 16802, USA
[12] European Southern Observatory, D-85748 Garching bei München, Germany
[13] Department of Astronomy, Harvard University, Cambridge, MA 02138, USA
[14] Jet Propulsion Laboratory, California Institute of Technology, Pasadena, CA 91109, USA
[15] Dr. Karl-Remeis-Sternwarte and ECAP, University of Erlangen-Nuremberg, D-96049 Bamberg, Germany
Received 2015 April 22; accepted 2015 May 9; published 2015 June 15

ABSTRACT

We present spectral analysis of *Nuclear Spectroscopic Telescope Array* and *Swift* observations of Cep X-4 during its outburst in 2014. We observed the source once during the peak of the outburst and once during the decay, finding good agreement in the spectral shape between the observations. We describe the continuum using a power law with a Fermi–Dirac cutoff at high energies. Cep X-4 has a very strong cyclotron resonant scattering feature (CRSF) around 30 keV. A simple absorption-like line with a Gaussian optical depth or a pseudo-Lorentzian profile both fail to describe the shape of the CRSF accurately, leaving significant deviations at the red side of the line. We characterize this asymmetry with a second absorption feature around 19 keV. The line energy of the CRSF, which is not influenced by the addition of this feature, shows a small but significant positive luminosity dependence. With luminosities between (1–6) $\times$ 10^{36} erg s^{-1}, Cep X-4 is below the theoretical limit where such a correlation is expected. This behavior is similar to Vela X-1 and we discuss parallels between the two systems.

Key words: accretion, accretion disks – radiation: dynamics – stars: neutron – X-rays: binaries – X-rays: individual (Cep X-4)

1. INTRODUCTION

Neutron star high-mass X-ray binaries, i.e., neutron stars accreting from an early-type stellar companion, typically show very high levels of variability in their X-ray emission. As the unabsorbed flux is directly related to the mass accretion rate, we can understand these changes as originating from variations of the latter. The physical conditions inside the accretion column, where most of the X-rays are produced, change with accretion rate. By sampling different luminosity levels we can obtain constraints on the geometry and physical processes in the accretion column. In particular, Be-star systems, where the stellar companion has a large circumstellar disk (e.g., Okazaki & Negueruela 2001), are ideally suited for studying the luminosity dependence of the X-ray spectrum, as they show weeks- to months-long outbursts that can cover more than two orders of magnitude in luminosity.

Many accreting neutron stars show prominent cyclotron resonant scattering features (CRSFs). CRSFs are produced by resonant scattering of photons off electrons moving perpendicular to the magnetic field. The electrons are quantized on Landau levels that energies depend directly on the local magnetic field, and therefore make the observed energy of the CRSF a direct tracer of the B-field (see, e.g., Schönherr et al. 2007 and references therein). With a variable accretion rate the cyclotron line production region can move along the accretion column, sampling different magnetic fields. A precise measurement of the CRSF therefore probes the accretion geometry of a source.

According to theoretical calculations, a strongly asymmetric shape of the fundamental line is predicted, with significant emission wings (e.g., Yahel 1979; Araya & Harding 1996, 1999; Isenberg et al. 1998; Araya-Góchez & Harding 2000; Schönherr et al. 2007; Schwarm 2010, among others). The shape is thereby strongly dependent on the accretion geometry and the underlying X-ray continuum. The asymmetry originates from photon-spawning,where electrons excited to higher harmonic Landau levels cascading back to the ground state and emitting photons close to the fundamental line energy (Schönherr et al. 2007).

Observationally, however, only very few of the approximately 25 known CRSF sources show any evidence for a deviation from very simply shaped fundamental lines. In GX 301–2, Kreykenbohm (2004) found marginal evidence for an asymmetric profile at certain pulse phases using *RXTE* data, but the statistics did not allow for a detailed description of the feature. Pottschmidt et al. (2005) and Nakajima et al. (2010) showed that the fundamental line in V0332+53 is better described by two absorption-like lines at almost the same energy, but with different widths. Iwakiri et al. (2012) claimed the detection of a CRSF in emission rather than absorption at

certain phases of 4U 1626–67, using *Suzaku* data. This feature might lead to a complex line profile in the phase-averaged data, but their data did not provide a high enough quality to measure it.

Among the six CRSF sources studied with the *Nuclear Spectroscopic Telescope Array* (*NuSTAR*; Harrison et al. 2013) so far, none show significant deviations from a Gaussian or Lorentzian optical depth profile (Fürst et al. 2013, 2014a, 2014b; Bellm et al. 2014; Tendulkar et al. 2014; Bhalerao et al. 2015). A detailed study of Her X-1 revealed good agreement in the line profile between *NuSTAR* and *Suzaku*, and put the most stringent limits on possible emission wings to date (Fürst et al. 2013).

The Be HXMB Cep X-4 has a CRSF around 30 keV, which is ideally suited to be studied in detail with *NuSTAR*, as a result of the instruments unprecedented energy resolution as well as increased sensitivity above 10 keV compared to previous missions. Cep X-4 was discovered by *OSO 7* in 1972 (Ulmer et al. 1972) and again detected by *Ginga* in 1988 (Makino & Ginga Team 1988). During the 1988 outburst, regular pulsations with a pulse period around 66 s were discovered, and evidence for a CRSF around 30 keV was found (Koyama et al. 1991; Mihara et al. 1991). The optical counterpart was identified by Bonnet-Bidaud & Mouchet (1998), who measured a distance of 3.8 ± 0.6 kpc.

The most detailed spectral description to date is presented by McBride et al. (2007), who used *RXTE* data taken during an outburst in 2002. They confirm the CRSF around 30.7 keV and describe the continuum with an absorbed power law with a Fermi–Dirac cutoff. By monitoring the source over the outburst they find a hardening of the broadband spectrum with luminosity, but the data quality does not allow the investigation of the dependence of the CRSF energy on luminosity. McBride et al. (2007) also show that the pulse profile changes significantly as a function of luminosity, confirming the results by Mukerjee et al. (2000), who use *RXTE* and Indian X-ray Astronomy Experiment data.

The rest of the Letter is organized as follows: in Section 2 we detail the data reduction, and in Section 3 we present the spectral analysis. Section 4 discusses and summarizes our results and concludes this Letter.

2. OBSERVATIONS AND DATA REDUCTION

In 2014 June MAXI detected renewed activity from Cep X-4 (Nakajima et al. 2014), and *Swift* performed pointed X-ray Telescope (XRT) observations after an automatic BAT trigger (Evans et al. 2014). Özbey-Arabacı et al. (2014) performed optical observations and found evidence for a strong Be-disk, expected to occur with the onset of the X-ray activity. We triggered *NuSTAR* observations and observed Cep X-4 twice, on 2014 June 18–19 (MJD 56826.92–56827.84, ObsID 80002016002, observation 1) close to the maximum of the outburst and on 2014 July 1–2 (MJD 56839.43–56840.31, ObsID 80002016004, observation 2) during the decline. Both *NuSTAR* observations were supported by *Swift*/XRT snapshots (ObsIDs 00080436003 and 00080436004, respectively). Figure 1 shows the light curves of *Swift*/BAT and MAXI, and the average count-rate of the *NuSTAR* observations.

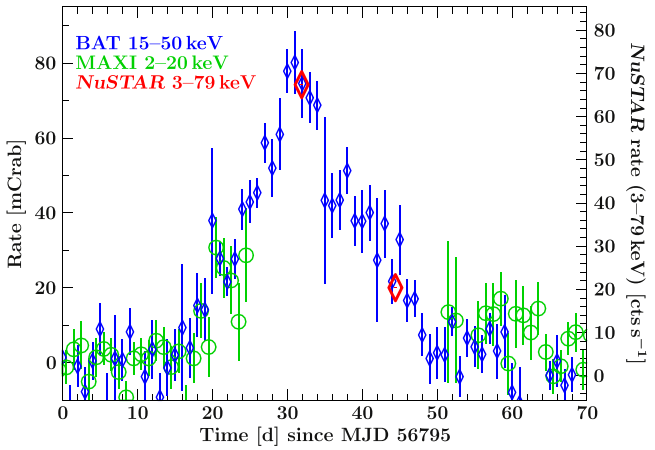

Figure 1. Light curve of the 2014 outburst of Cep X-4 as observed with *Swift*/BAT (blue diamonds), MAXI (green circles), and *NuSTAR* (red diamonds). All rates were rescaled to mCrab in the respective energy band. The right hand *x*-axis gives the measured count-rates for the *NuSTAR* data. MAXI did not take data during the maximum of the outburst.

2.1. NuSTAR

We extracted *NuSTAR* data using the standard `nupipeline` software v1.4.1 as distributed with HEASOFT 6.16. We used CALDB v20150316, taking a time-dependent gain change into account. Standard screening of the data resulted in good exposure times of 40.5 ks for observation 1 and 41.2 ks for observation 2. We extracted source spectra separately for FPMA and FPMB from a circular region with a radius of 120″ centered at the J2000 coordinates. The background spectra were extracted from the opposite corner of the *NuSTAR* field of view from a circular region with 90″ radius.

Spectra were modeled with the Interactive Spectral Interpretation System (ISIS; Houck & Denicola 2000) v1.6.2–30 and errors are given at the 90% confidence level unless otherwise noted. The data were rebinned within ISIS to a signal-to-noise ratio (S/N) of eight between 3.2–45 keV and an S/N of three above that, binning at least two channels together. While the *NuSTAR* calibration is nominally good down to 3 keV we choose to ignore the first few bins in order to allow *Swift*/XRT to drive the model at the lowest energies. We include data up to 60 keV, where they become background dominated.

2.2. Swift/XRT

Data from the *Swift*/XRT (Burrows et al. 2005) were extracted following the steps outlined in the *Swift* user's guide (Capalbi et al. 2005) using HEASOFT 6.16. Observation 1 (MJD 56826.94–56826.956) was performed in windowed timing mode, and we extracted the source spectrum from a rectangular region with 45″ length perpendicular to the read-out direction. The background was extracted from similar regions on both sides of the source location. After standard screening we obtained a good exposure time of 1.0 ks.

Observation 2 (MJD 56839.462–56839.531) was performed in photon counting mode and was heavily piled-up. Following the procedure described in the XRT data analysis guide[16] we determined that an annulus extraction region with inner radius 12″ and outer radius 60″ removes most pile-up while still

[16] http://www.swift.ac.uk/analysis/xrt/pileup.php

providing a good S/N spectrum. The background was estimated from a large region south–east of the source. The observation resulted in 1.6 ks of good exposure time. Both *Swift*/XRT spectra were rebinned to an S/N of six throughout the used energy range of 0.8–10 keV.

3. SPECTRAL ANALYSIS

As McBride et al. (2007) demonstrate, the hard X-ray continuum of Cep X-4 is well described by an absorbed power law with a Fermi–Dirac cutoff (Tanaka 1986) of the form

$$F(E) \propto E^{-\Gamma} \times \left(1 + \exp\left(\frac{E - E_{\rm cut}}{E_{\rm fold}}\right)\right)^{-1}. \quad (1)$$

To that continuum, McBride et al. (2007) add a CRSF modeled by a multiplicative absorption line[17] with a Gaussian optical depth profile (`gabs` in XSPEC) and a narrow additive fluorescent Fe Kα line. We apply this same model to both observations separately, modeling *Swift*/XRT, *NuSTAR*/FPMA, and FPMB simultaneously and allowing for a cross-calibration constant relative to FPMA for FPMB and XRT ($C_{\rm FPMB}$ and $C_{\rm XRT}$). We use the `phabs` absorption model with abundances by Wilms et al. (2000) and cross-sections by Verner et al. (1996).

The model results in an unacceptable fit for both observations (χ^2/dof = 2275/1087 = 2.09 for observation 1 and χ^2/dof = 1128/675 = 1.67 for observation 2) with strong residuals below 10 keV. We therefore add a blackbody component with $kT_{\rm BB} \approx 1$ keV that improves the fit significantly. We obtain χ^2/dof = 1324/1085 = 1.22 for observation 1 and χ^2/dof = 802/673 = 1.19 for observation 2. The residuals of observation 1 for this model are shown in Figure 2 (b).

As can be seen in Figure 2(b), the residuals still show some structure between 10–20 keV that is not modeled by the CRSF. We therefore add another multiplicative absorption line with a Gaussian optical depth profile. This addition provides a significant improvement and results in a good fit, with χ^2/dof = 1215/1082 = 1.12 for observation 1 and χ^2/dof = 776/670 = 1.16 for observation 2. The energy of the CRSF does not change significantly when adding the second absorption model, which is found to be around $E_{\rm abs} \approx 19$ keV in both observations. The residuals to this best-fit model are shown in Figures 2(c) and (d) for observation 1 and 2, respectively, and the best-fit parameters are given Table 1.

Using two lines with Gaussian optical depth profiles describes the shape of the CRSF in both observations very well. Using a pseudo-Lorentzian profile instead (modeled by the `cyclabs` model) results in a very similar fit and also requires a second absorption feature. The line energies are about 2 keV lower, consistent with the expected difference between the models (see, e.g., Staubert et al. 2014). Our model is therefore insensitive to the slight differences in shape between the two profiles, similar to results obtained for Her X-1 (Fürst et al. 2013) and V 0332 + 35 (Pottschmidt et al. 2005; Nakajima et al. 2010).

The CRSF energy shows small but statistically significant variations with luminosity, decreasing from

[17] We note that while a CRSF is produced by resonant scattering, not absorption, a possible parametrization is the same as for the latter.

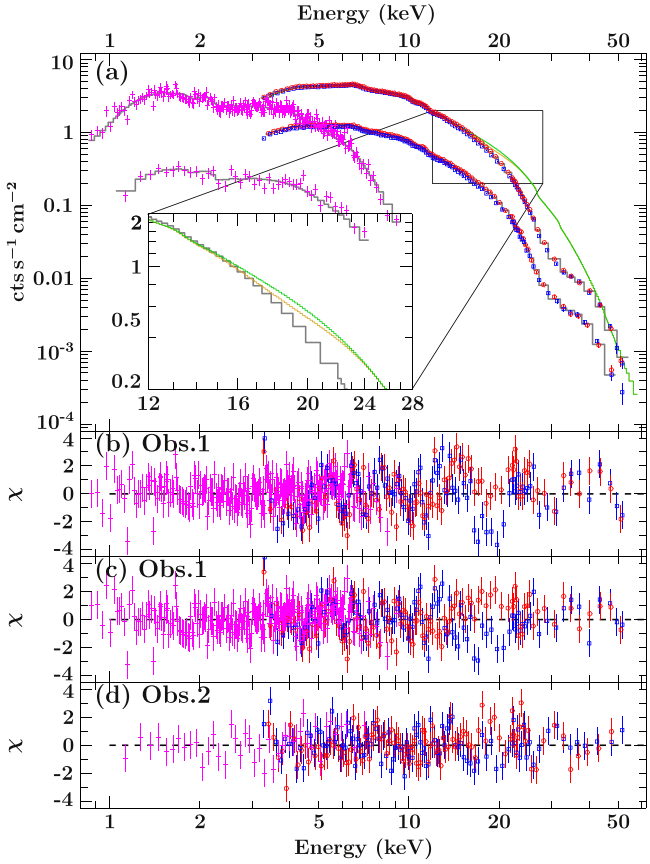

Figure 2. (a) Count spectra and best-fit models of both observations of Cep X-4. *Swift*/XRT data are shown in magenta, *NuSTAR*/FPMA data in red, and *NuSTAR*/FPMB data in blue. The best-fit model is shown in gray, the model evaluated without the absorption lines in green, and the model with only the primary CRSF in orange. The inset shows a zoom on the red edge of the CRSF in observation 1. (b) Residuals of observation 1 to a FDcut model with only one absorption line, (c) residuals of observation 1 to the best-fit model, (d) residuals of observation 2 to the best-fit model. Data were rebinned for plotting purposes.

$E_{\rm Obs\,1} = 30.39^{+0.17}_{-0.14}$ keV in the first observation to $E_{\rm Obs\,2} = 29.42^{+0.27}_{-0.24}$ keV in the second observation. This behavior is qualitatively the same with or without the second absorption feature. In order to rule out the possibility that small changes in the continuum parameters influence the measured energy of the CRSF, we performed a simultaneous fit of both data sets. This was possible as the continuum parameters (besides the normalization) do not change significantly between the two observations. In the simultaneous fit, the photon index Γ, the folding energy $E_{\rm fold}$, the cutoff energy $E_{\rm cut}$, the absorption column $N_{\rm H}$, and the Fe Kα line parameters are tied between both data sets. We obtain very similar results with respect to the two absorption features and the blackbody component, in particular the luminosity dependence of the CRSF energy is seen with the same significance and both observations require a second absorption feature.

In order to further investigate the choice of the continuum on the shape and energy of the CRSF, we also model the data with an NPEX model (Mihara 1995), in which we fix the secondary power-law index to $\Gamma_2 = -2$. We obtain a very similar statistical quality of fit and consistent parameters. The energy of the line is fitted to $E_{\rm Obs\,1} = 30.59^{+0.13}_{-0.15}$ keV and $E_{\rm Obs\,2} = 29.43^{+0.23}_{-0.22}$ keV. The secondary absorption feature is

Table 1
Parameters of the Best-fit Fermi–Dirac Cutoff Model for Both Observations

Parameter	Observation 1	Observation 2
$N_{\rm H}$ (10^{22} cm^{-2})	$1.05^{+0.11}_{-0.12}$	1.41 ± 0.25
$A_{\rm cont}$ [a]	$0.061^{+0.008}_{-0.010}$	$0.021^{+0.004}_{-0.005}$
Γ	$0.83^{+0.07}_{-0.11}$	$0.96^{+0.09}_{-0.14}$
$E_{\rm cut}$ (keV)	24 ± 4	25 ± 4
$E_{\rm fold}$ (keV)	$5.7^{+0.5}_{-0.6}$	$5.7^{+0.6}_{-0.8}$
$E_{\rm CRSF}$ (keV)	$30.39^{+0.17}_{-0.14}$	$29.42^{+0.27}_{-0.24}$
$\sigma_{\rm CRSF}$ (keV)	5.8 ± 0.4	4.9 ± 0.4
$d_{\rm CSRF}$ [b] (keV)	20^{+5}_{-4}	$16.6^{+4.0}_{-3.0}$
$E_{\rm abs}$ (keV)	$19.0^{+0.5}_{-0.4}$	18.5 ± 0.7
$\sigma_{\rm abs}$ (keV)	2.5 ± 0.4	2.1 ± 0.5
$d_{\rm abs}$ [b] (keV)	$0.60^{+0.24}_{-0.17}$	$0.37^{+0.21}_{-0.15}$
A (Fe Kα)[a]	$\left(1.39^{+0.16}_{-0.14}\right) \times 10^{-3}$	$\left(2.8^{+0.8}_{-0.6}\right) \times 10^{-4}$
σ (Fe Kα) (keV)	0.42 ± 0.05	$0.34^{+0.12}_{-0.10}$
E (Fe Kα)(keV)	$6.474^{+0.030}_{-0.032}$	$6.39^{+0.06}_{-0.07}$
$A_{\rm BB}$ [c]	$\left(2.22^{+0.41}_{-0.29}\right) \times 10^{-3}$	$\left(7.3^{+1.7}_{-1.3}\right) \times 10^{-4}$
$kT_{\rm BB}$ (keV)	$0.899^{+0.030}_{-0.031}$	0.96 ± 0.06
$C_{\rm FPMB}$	1.0319 ± 0.0019	1.023 ± 0.004
$C_{\rm XRT}$	0.962 ± 0.019	0.91 ± 0.05
χ^2/dof	1215.83/1082	776.35/670
$\chi^2_{\rm red}$	1.124	1.159

Notes.
[a] In photons keV^{-1} s^{-1} cm^{-2} at 1 keV.
[b] Line depth, optical depth=$d/(\sigma\sqrt{2\pi})$.
[c] In 10^{39} erg s^{-1} for a source at 10 kpc.

also clearly visible in the residuals and its addition leads to a similar improvement in terms of χ^2.

4. DISCUSSION

We have presented simultaneous *Swift* and *NuSTAR* observations at two different luminosities taken during an outburst of Cep X-4 in 2014 June and July. We describe the broad-band spectrum with a power law attenuated by absorption and a Fermi–Dirac cutoff. We find that the continuum does not change significantly between the observations but that the CRSF shows complex behavior.

4.1. Shape of the CRSF

We have shown that to accurately describe the hard X-ray spectrum of Cep X-4 we require a second absorption feature in addition to the prominent CRSF around 30 keV. If this feature were the fundamental line, it would imply a lower magnetic field strength than previously suggested. That is, however, unlikely as we expect the ratio of the fundamental and first harmonic line energy to be close to 2, while we measure ≈1.56. Other sources also show deviations from the expected factor, however, they are typically much smaller (<10%; e.g., Pottschmidt et al. 2005; Müller et al. 2013). The deviation we observe is too large to be explained by relativistic effects (Mészáros 1992).

The second feature is also unlikely to result from sampling different accretion columns or different regions. If that were the case, the strength of the 30 keV line would be difficult to explain as this scenario implies that the line should only be present at some phase intervals. In order to further investigate this we will present results of phase-resolved spectroscopy in a separate paper (V. Bhalerao et al. 2015, in preparation). The production of two CRSFs of such different energies in different accretion columns would also indicate a strong deviation from a simple dipole magnetic field, which is not expected (see Nishimura 2005 for a discussion of the influence of multipole fields on the CRSF).

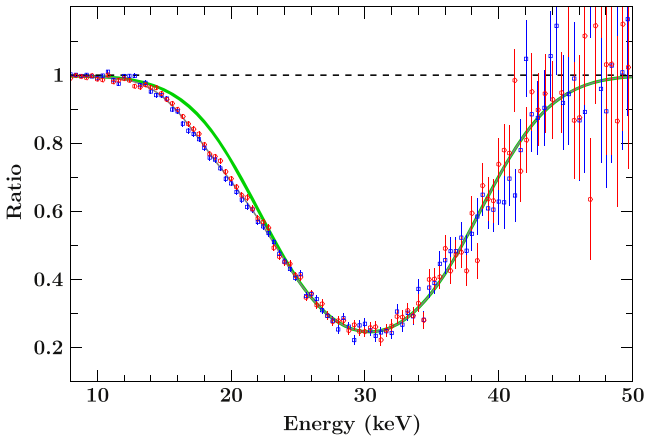

Figure 3. Residuals of observation 1 in terms of data-to-model ratio. The ratio was calculated by setting the strength of both absorption features to zero. FPMA data are shown in red, FPMB in blue. The best-fit model is shown in gray. The green line shows the ratio when only setting the second absorption feature to zero, i.e., when assuming a symmetric line profile. The data were strongly rebinned for the plot.

The most likely explanation for the second absorption feature is a deviation of the shape of the CRSF from a smooth Gaussian or Lorentzian profile. This deviation is highlighted in Figure 3, where we plot the data-to-model ratio using the best-fit model with both lines removed. We superimpose the ratio between this model and the best-fit model with the secondary feature removed, which implicitly shows a simple symmetric line profile. From this ratio the data clearly deviate at the red wing. A similar deviation might be present on the blue side, however, the data quality does not us allow to constrain this. Adding a feature there with a similar optical depth does not change the statistical quality of the fit significantly.

Prominent emission wings would be the most obvious explanation for deviations from a smooth line. However, such emission wings typically require a harder spectrum than we observe to spawn enough photons to become significant (Schönherr et al. 2007). On the other hand, depending on geometry and optical depth, photon spawning can lead to distorted shapes of the scattering trough without creating measurable emission wings (Schwarm 2010). As can be seen in the inset of Figures 2 and 3, the second absorption feature is located exactly at the energy where the primary CRSF starts to produce significant deviations from the continuum spectrum, supporting this interpretation.

4.2. Luminosity Dependence of the CRSF

Thanks to *NuSTAR*'s energy resolution, we are able to constrain the centroid of the line energy to better than ±0.3 keV. This allowed us to measure a significant change between the two observations, which appears to be correlated with luminosity. To highlight that correlation and put it into context, we show the CRSF energy as a function of luminosity in Figure 4 for different sources. The energy decreases with

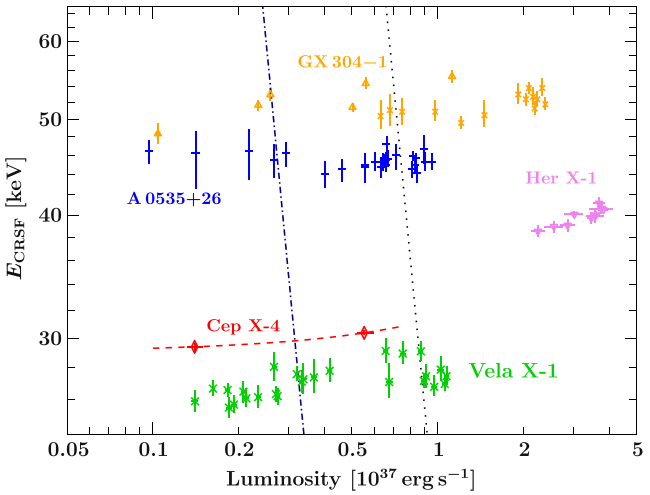

Figure 4. Dependence of the CRSF energy on luminosity for different sources. Cep X-4 data are plotted as red diamonds with a best-fit linear correlation superimposed (dashed line). Vela X-1 data (green asterisk) are from Fürst et al. (2014a) and show the energy of the first harmonic CRSF divided by 2. A 0535+26 data (blue crosses) are from Caballero et al. (2007), Her X-1 data (magenta down-pointing triangles) are from Staubert et al. (2007), and GX 304–1 (orange up pointing triangles) are from Yamamoto et al. (2011) and Klochkov et al. (2012). The dotted line indicates the original Coulomb stopping luminosity presented by Becker et al. (2012) and the dotted–dashed line indicates the updated values for Vela X-1 (Fürst et al. 2014a).

declining flux, leading to a positive correlation between luminosity and CRSF energy. The luminosity of Cep X-4 is between (1–6) × 10^{36} erg s^{-1} for a distance of 3.8 kpc, which is below the theoretical limit for the formation of a shock in the accretion column (Becker et al. 2012). We therefore expect a constant CRSF energy uncorrelated with luminosity, as observed in A 0535+26 (Caballero et al. 2007, but see Sartore et al. 2015 for indications of a correlation). In recent *NuSTAR* observations of Vela X-1, Fürst et al. (2014a) show that this source also has a significant positive correlation between CRSF energy and luminosity at luminosities below 10^{37} erg s^{-1}.

Fürst et al. (2014a) follow the calculations of Becker et al. (2012) but allow for wind-accretion instead of disk-accretion and assume a massive neutron star (around 2 $M_{\odot}$ in Vela X-1). This results in a narrower accretion column than assumed in Becker et al. (2012), which in turn decreases the luminosity threshold required for shock formation significantly, moving the measured luminosities of Vela X-1 partially above it (see the dotted–dashed line in Figure 4). Cep X-4 also crosses this adopted line, although the mass of the neutron star in this system is not known. Additionally, Cep X-4 is a Be-system, and so we expect that the accreted matter forms a temporary accretion disk around the neutron star, which leads to a different accretion geometry than in purely wind accreting systems (e.g., Ghosh & Lamb 1979; Okazaki et al. 2013). If the accretion geometry could be constrained, this correlation might indicate that the neutron star in Cep X-4 is also massive, with $M > 2\,M_{\odot}$.

4.3. Summary

NuSTAR has revealed two new interesting features of the CRSF in Cep X-4: a distorted profile and a luminosity dependence of the line's energy. This makes Cep X-4 the first system where a significant deviation from a symmetric line profile has been measured in the phase averaged spectrum and the second system where a positive correlation between CRSF energy and luminosity has been found at luminosities below 10^{37} erg s^{-1}. The latter discovery challenges the current understanding of the accretion column geometry, as the line forming region is expected to be at the neutron star surface and therefore independent of luminosity.

The discovery of a complex line profile on the other hand is a good qualitative confirmation of theoretically predicted line-profiles when taking photon-spawning and magnetic field gradients into account (e.g., Nishimura 2005; Schönherr et al. 2007). By combining detailed calculations of the line profile with sophisticated light bending calculations, it should be possible to improve our understanding of the emission geometry in Cep X-4 and other neutron star systems.

We thank the anonymous referee for valuable comments. This work was supported under NASA contract No. NNG08FD60C, and made use of data from the *NuSTAR* mission, a project led by the California Institute of Technology, managed by the Jet Propulsion Laboratory, and funded by the National Aeronautics and Space Administration. We thank the *NuSTAR* Operations, Software and Calibration teams for support with the execution and analysis of these observations. This research has made use of the *NuSTAR* Data Analysis Software (NuSTARDAS) jointly developed by the ASI Science Data Center (ASDC, Italy) and the California Institute of Technology (USA).

REFERENCES

Araya, R. A., & Harding, A. K. 1996, A&AS, 120, C183
Araya, R. A., & Harding, A. K. 1999, ApJ, 517, 334
Araya-Góchez, R. A., & Harding, A. K. 2000, ApJ, 544, 1067
Becker, P. A., Klochkov, D., Schönherr, G., et al. 2012, A&A, 544, A123
Bellm, E. C., Fürst, F., Pottschmidt, K., et al. 2014, ApJ, 792, 108
Bhalerao, V., Romano, P., Tomsick, J., et al. 2015, MNRAS, 447, 2274
Bonnet-Bidaud, J. M., & Mouchet, M. 1998, A&A, 332, L9
Burrows, D. N., Hill, J. E., Nousek, J. A., et al. 2005, SSRv, 120, 165
Caballero, I., Kretschmar, P., Santangelo, A., et al. 2007, A&A, 465, L21
Capalbi, M., Perri, M., Saija, B., Tamburelli, F., & Angelini, L. 2005, The SWIFT XRT Data Reduction Guide, version 1.2
Evans, P. A., Beardmore, A. P., Krimm, H. A., & Lien, A. Y. 2014, ATel, 6243
Fürst, F., Grefenstette, B. W., Staubert, R., et al. 2013, ApJ, 778, 69
Fürst, F., Pottschmidt, K., Wilms, J., et al. 2014a, ApJ, 780, 133
Fürst, F., Pottschmidt, K., Wilms, J., et al. 2014b, ApJL, 784, L40
Ghosh, P., & Lamb, F. K. 1979, ApJ, 232, 259
Harrison, F. A., Craig, W., Christensen, F., et al. 2013, ApJ, 770, 103
Houck, J. C., & Denicola, L. A. 2000, in Astronomical Data Analysis Software and Systems IX, Vol. 216, ed. N. Manset, C. Veillet, & D. Crabtree (San Francisco, CA: ASP), 591
Isenberg, M., Lamb, D. Q., & Wang, J. C. L. 1998, ApJ, 505, 688
Iwakiri, W. B., Terada, Y., Mihara, T., et al. 2012, ApJ, 751, 35
Klochkov, D., Doroshenko, V., Santangelo, A., et al. 2012, A&A, 542, L28
Koyama, K., Kawada, M., Tawara, Y., et al. 1991, ApJL, 366, L19
Kreykenbohm, I. 2004, PhD thesis, Eberhard-Karls-Univ. Tübingen
Makino, F., & GINGA Team 1988, IAUC, 4575, 1
McBride, V. A., Wilms, J., Kreykenbohm, I., et al. 2007, A&A, 470, 1065
Mészáros, P. 1992, High-energy Radiation from Magnetized Neutron Stars (Chicago, IL: Univ. Chicago Press)
Mihara, T. 1995, PhD thesis, Dept. of Physics, Univ. of Tokyo
Mihara, T., Makishima, K., Kamijo, S., et al. 1991, ApJL, 379, L61
Mukerjee, K., Agrawal, P. C., Paul, B., et al. 2000, A&A, 353, 239
Müller, S., Ferrigno, C., Kühnel, M., et al. 2013, A&A, 551, A6
Nakajima, M., Mihara, T., & Makishima, K. 2010, ApJ, 710, 1755
Nakajima, M., Negoro, H., Kawagoe, A., et al. 2014, ATel, 6212
Nishimura, O. 2005, PASJ, 57, 769
Okazaki, A. T., Hayasaki, K., & Moritani, Y. 2013, PASJ, 65, 41
Okazaki, A. T., & Negueruela, I. 2001, A&A, 377, 161

Özbey-Arabacı, M., Camero-Arranz, A., Fabregat, J., Ozcan, H. B., & Peris, V. 2014, ATel, 6265
Pottschmidt, K., Kreykenbohm, I., Wilms, J., et al. 2005, ApJL, 634, L97
Sartore, N., Jourdain, E., & Roques, J.-P. 2015, ApJ, in press (arXiv:1504.03726)
Schönherr, G., Wilms, J., Kretschmar, P., et al. 2007, A&A, 472, 353
Schwarm, F. 2010, Diploma thesis, Dr Karl Remeis-Sternwarte Bamberg and ECAP, FAU Erlangen-Nürnberg
Staubert, R., Klochkov, D., Wilms, J., et al. 2014, A&A, 572, A119
Staubert, R., Shakura, N. I., Postnov, K., et al. 2007, A&A, 465, L25
Tanaka, Y. 1986, in Radiation Hydrodynamics in Stars and Compact Objects, Vol. 255, ed. D. Mihalas & K.-H. A. Winkler (New York: Springer), 89
Tendulkar, S. P., Fürst, F., Pottschmidt, K., et al. 2014, ApJ, 795, 154
Ulmer, M. P., Baity, W. A., Wheaton, W. A., & Peterson, L. E. 1972, ApJL, 178, L121
Verner, D. A., Ferland, G. J., Korista, K. T., & Yakovlev, D. G. 1996, ApJ, 465, 487
Wilms, J., Allen, A., & McCray, R. 2000, ApJ, 542, 914
Yahel, R. Z. 1979, ApJL, 229, L73
Yamamoto, T., Sugizaki, M., Mihara, T., et al. 2011, PASJ, 63, 751